JACS
JOURNAL OF THE AMERICAN CHEMICAL SOCIETY

Article

pubs.acs.org/JACS

Ions from Solution to the Gas Phase: A Molecular Dynamics Simulation of the Structural Evolution of Substance P during Desolvation of Charged Nanodroplets Generated by Electrospray Ionization

Doyong Kim,[†] Nicole Wagner,[†] Kerry Wooding,[†,§] David E. Clemmer,[‡] and David H. Russell*[,†]

[†]Department of Chemistry, Texas A&M University, College Station, Texas 77843, United States

[‡]Department of Chemistry, Indiana University, Bloomington, Indiana 47405, United States

Supporting Information

ABSTRACT: Molecular dynamics (MD) simulations are used to model changes in the conformational preferences of a model peptide during the transition from a hydrated environment (charged nanodroplet generated by electrospray ionization) to the solvent-free peptide ion. The charged droplet consists of ~2400 water molecules, 22 hydronium ions, and 10 chloride and contains a single Substance P (SP) $[SP + 3H]^{3+}$ ion (SP^{3+}; amino acid sequence RPKPQQFFGLM-NH_2). Initially, droplet shrinkage involves a combination of solvent evaporation and ejection of excess charge, primarily hydronium ions. Further droplet shrinkage leads to a series of fission events, which includes the loss of some Cl^- ions. SP^{3+} ions adapt to the smaller size droplet through small conformational changes that result in coiling of the hydrophobic C-terminus of the peptide on or near the droplet surface, intramolecular interactions involving the hydrophilic N-terminus of the peptide, and water-mediated interactions between the SP^{3+} ion and H_3O^+ and Cl^- ions. Calculated collision cross sections (CCS) for SP^{3+} ions at various stages of desolvation are consistent with the results obtained from cryogenic ion mobility-mass spectrometry (cryo-IM-MS) measurements. Specifically, early in the decay of the charged droplet SP^{3+} ions favor an extended conformation, whereas a compact conformer is favored during the final stages of dehydration.

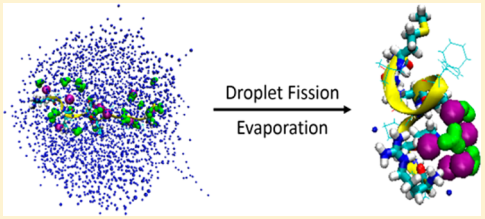

INTRODUCTION

Native-electrospray ionization (n-ESI) has provided new dimensions to biological mass spectrometry, making possible transitions from the determination of primary (1°) structure to studies of higher order (2°, 3°, and 4°) structure, thereby opening new vistas in the field of structural biology.[1−3] The use of gas-phase structure determination approaches as probes of solution-phase biomolecule structure necessitates understanding how solution-phase structure(s) are influenced as they transition from solution to solvent-free, gas-phase ions.[4,5] While early fundamental studies of electrospray ionization (ESI) were focused on issues related to the generation of ions from charged liquid droplets, the growing emphasis on structure determination using mass spectrometry raises new questions, specifically the question posed by Breuker and McLafferty, "for how long, under what conditions, and to what extent, can solution structure be retained without solvent?"[6] Studies by Chen et al. partially addressed this question; they presented evidence that ubiquitin (an ordered protein)[7,8] and apo- and partially metalated metallothionein-2A (a disordered protein)[9] ions formed using "native-state" ESI are indeed formed as native or "native-like" conformers,[9,10] but great care must be taken in order to preserve the nascent ion population, especially for flexible/disordered proteins.

ESI of large biomolecules has inspired much experimental and theoretical research aimed at understanding the underlying mechanism(s) of ion formation.[11−15] The two most widely accepted models used to describe ESI ion formation are (1) the charge residue model (CRM), where nanodroplets that contain a single analyte ion evaporate to dryness and the charge on the droplet is transferred to the analyte,[14,16−21] and (2) the ion evaporation model (IEM), which assumes the surface charge density of a droplet is sufficiently high to eject a small hydrated ion that resides on or near the surface of the droplet.[14,19,20,22,23] Hogan et al. combined the elements of the CRM and IEM ionization mechanisms as the charged-residue/field-emission model.[24] Consta et al. described a mechanism whereby macromolecule ions are extruded from the charge droplet,[25] and Konermann et al. described a similar chain ejection model (CEM), which they propose as a mechanism for ionization of disordered polymers.[26,27] Molecular dynamics (MD) simulations have provided tremendous insights and detailed models for understanding the transition from small (nm diameter) droplets to the solvent-free ion,[28] and a recent review by Consta et al. describes more rigorous treatment of the ESI mechanism and the factors that determine droplet fission.[19,25,29]

Our understanding of the transition from solution to the solvent-free, gas-phase ion is largely derived from MD simulations, but there exists a paucity of experimental evidence

Received: October 13, 2016
Published: January 27, 2017

ACS Publications © 2017 American Chemical Society

DOI: 10.1021/jacs.6b10731
J. Am. Chem. Soc. 2017, 139, 2981−2988

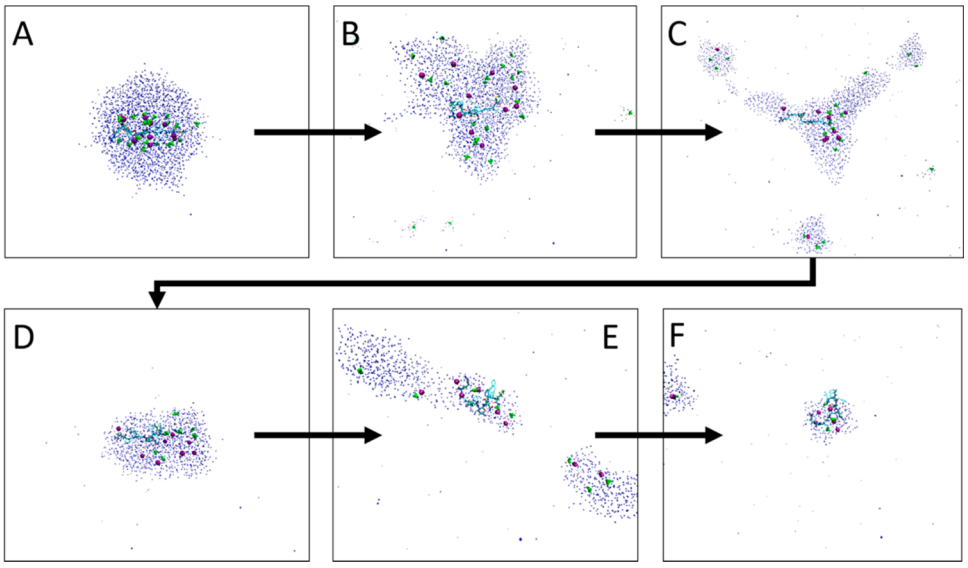

Figure 1. Snapshots of the early stages of the desolvation process of a droplet containing SP^{3+}, chloride, and hydronium ions from a single simulation shown after (A) 0 ps, (B) ~400 ps, (C) ~560 ps, (D) ~825 ps, (E) ~1500 ps, and (F) ~1550 ps.

to validate the models describing this process, especially how late desolvation processes affect conformational preferences of the analyte ions.[30] Cryo-ion mobility-mass spectrometry (cryo-IM-MS) provides a means for direct observation of the effects of hydration on the size/shape of biomolecule ions. This approach provides a means to experimentally measure the size and abundances of hydrated ions of the type $[M + nH]^{n+}\cdot(H_2O)_x$, where x ranges from a few hundred water molecules to only the remnant water molecules interacting with the most hydrophilic functional groups, and finally to the solvent-free, gas-phase ion.[31−34] In the case of the amphipathic peptide SP (RPKPQQFFGLM-NH_2) $[M + 3H]^{3+}$ ions, the transition from solution to the gas phase occurs via a series of dehydration steps that can be traced to a single, compact peptide ion conformer.[31,33] Similar structural changes that occur late in the dehydration reactions have been observed for ionic water clusters $(H^+(H_2O)_n$, dialkylammonium cations, site-specific mutants of substance P (Q5A, Q6A, and Q5,6A), and the reverse sequence of substance P (MLGFFQQPKPR-NH_2).[32,33] Here, we use MD simulations to examine the effects of the changing solvent environment on the conformation of the SP^{3+} ion as the droplet size decreases by fission events, ejection of small ionic water clusters, and evaporation of single water molecules. The results from MD simulations suggest that interactions of SP^{3+} ions with H_2O, H_3O^+, and Cl^- (introduced as a simple counterion) influence intramolecular interactions that lead to kinetic trapping of the compact conformer; these effects are also examined by ambient ESI-IM-MS.

EXPERIMENTAL SECTION

Molecular Dynamics Simulations. MD simulations were conducted on a 176-core SGI Altix 450 cluster at the Texas A&M University Laboratory for Molecular Simulation. The AMBER 11 molecular dynamics package and AMBER ff99SB force fields were used in this study. GAUSSIAN 03 and RED III[35] were used to create custom amino acids that were not supported in AMBER. Hydronium ion parameters were obtained from results of Baaden et al.[36] All CCS values for the peptide ions were calculated using the MOBCAL trajectory method.[37,38]

All simulations were performed on a water droplet consisting of approximately 2400 TIP3P water molecules (with the exception of a single simulation droplet consisting of approximately 3400 water molecules), and the vacuum box size was set to ~230 Å. For all simulations, droplet energy minimization was performed and followed by 20 ps for droplet equilibration at 360 K. Trial desolvation simulations were performed to evaluate the effects of droplet temperature, charge, and electrostatic nonbonding cutoff on simulated droplet fission events, solvent evaporation, and overall droplet dynamics (see Supporting Information, Figures S1−S8). Simulations performed using a cutoff of 8 and 100 Å indicated only minor differences in overall droplet dynamics; consequently, a cutoff of 8 Å was used for all subsequent simulations in order to minimize computational cost. The Rayleigh limit for a droplet consisting of approximately 2400 TIP3P water molecules is ~13, as calculated using the surface tension of the TIP3P water model.[39,40] From the trial simulations, it was determined that an overall charge of 15+ would be used for all simulations. This decision was based on the fact that such droplets undergo some solvent evaporation prior to experiencing fission events consistent with that previously reported.[41,42] The temperature for each simulation was set to 360 K using a Langevin thermostat.[31] A temperature of 360 K (mimicking the capillary temperature of the cryo-IM-MS instrument and the source temperature of the ambient Waters Synapt G2) was chosen from the trial simulations for all subsequent simulations. In the final stages of dehydration, the rate of evaporation slowed dramatically, and the temperature was increased to 420 K.

The TIP3P model has limitations in that H_2O is treated as a static,[43] nonpolarizable ion[44] and the surface tension is lower than the real value for water.[40] Despite these differences, previous evaporation simulations using the TIP3P model indicate similar behavior when compared to other complex water models,[45] but the TIP3P model has the benefit of being less computationally expensive. The electrostatic nonbonded cutoff was set to 8 Å in order to minimize computational cost, and the vacuum simulation box size was set to ~230 Å.

Wilm estimated that an ESI droplet of 200 nm diameter generated from a solution containing 1 pmol/μL of analyte contains on average a single analyte molecule.[46] Therefore, each simulation was performed on a droplet containing a single SP^{3+} ion. Note that the N-terminus, R1, and K3 were protonated due to their high proton affinities and the use of acidic conditions.[47] In summary, a total of 12 MD simulations were performed on water droplets that contained a single SP^{3+} ion, 22 H_3O^+, and 10 Cl^- anions resulting in a total charge of 15+ within the droplet.

Three sets of four replicate MD simulations were carried out for droplets containing a SP^{3+} ion, H_3O^+, and Cl^-. The droplet for the first set of four simulations was constructed by placing the extended solution-phase conformer of SP^{3+} in the center of the droplet and randomly placing H_3O^+, and Cl^- near the peptide; all replicates for the first set of

DOI: 10.1021/jacs.6b10731
J. Am. Chem. Soc. 2017, 139, 2981−2988

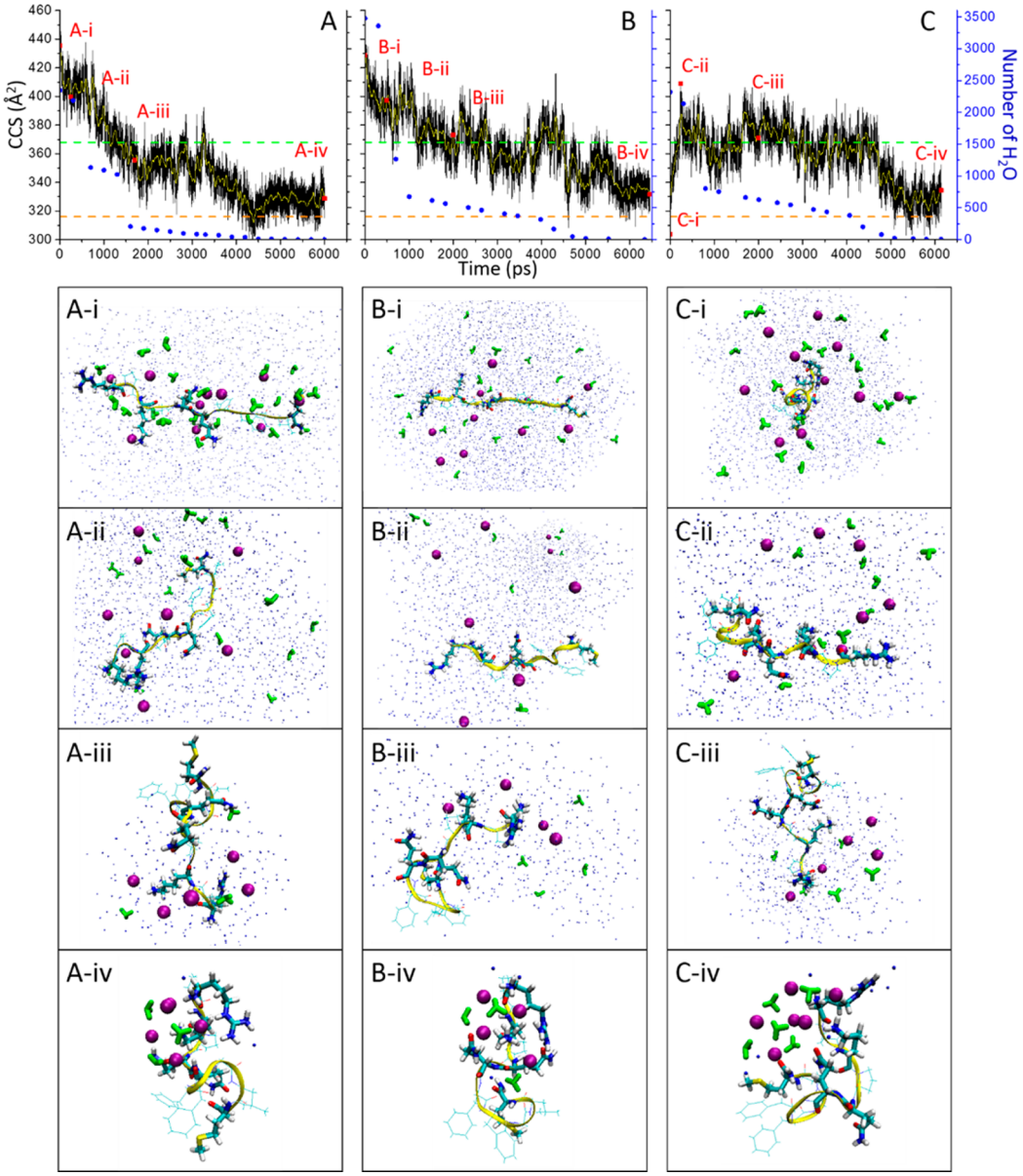

Figure 2. (A–C) Three plots showing the CCS of SP^{3+} (RPKPQQFFGLM-NH_2) ions (raw data, black line; smoothed, yellow line) and numbers of water molecules (blue points) vs time extracted from selected simulations. The experimentally determined CCS of SP^{3+} (316 and 368 $Å^2$) are also shown for reference (orange and green dash respectively). Note that simulations labeled A and B begin with an extended SP^{3+} ion conformation, and the simulation labeled C began with a compact conformer having a CCS of 316 $Å^2$. Structures labeled as i–iv depict representative snapshots of the simulations (A–C) from (i) the start of the simulation, (ii) initial peptide structural equilibration, (iii) hydrophobic side-chain surface coiling, and, finally, (iv) to the end of the simulation. Blue dots represent water molecules, purple spheres represent Cl^- ions, and H_3O^+ ions are shown in green.

simulations began with exactly identical ion locations (results of the set 1 shown in Figure S9A–D). The second set of four simulations was carried out using the same peptide structure, but each simulation was constructed using randomly placed H_3O^+, and Cl^- within the droplet (see Figure S9E–H). The final four simulations were performed starting with a droplet containing randomly placed Cl^- and H_3O^+ ions and a compact SP^{3+} ion with a CCS that is similar to the experimentally determined value for conformer A of 316 $Å^2$ (see Figure S9I–L).[31,48] The charge sites on the peptide were fixed on the most basic functional groups, *viz*. the N-terminus and the arginine and lysine side chains.

Sample Preparation. SP and melittin from honeybee venom (both from Sigma-Aldrich, St. Louis, MO, USA) were used without further purification. Each peptide was diluted to a concentration of 10 μM with 18 MΩ water, water/0.1% formic acid (98% w/w, Fluka), or water/0.1% hydrochloric acid (37.3% w/w, Fisher Scientific, Pittsburgh, PA, USA).

IM-MS Measurements. All cryogenic ESI-IM-MS data were acquired on a home-built instrument.[49−51] Note that a capillary voltage of 363 K and drift cell temperature of 85 K were used for each acquisition. All ambient ESI-IM-MS data were acquired using a Waters Synapt G2 HDMS instrument (Manchester, UK). The instrument was tuned to minimize collisional activation. The instrument conditions used were as follows: sample cone 10 V, extraction cone 1 V, trap bias 25 V, helium cell flow rate 200 mL/min, IMS nitrogen flow rate 50 mL/min.[9]

RESULTS AND DISCUSSION

Evolution of the ESI Droplet from MD Simulations. Consta et al. and Konermann et al. have performed desolvation simulations on charged droplets containing cations and anions to investigate the effect of their ions on the ESI mechanism.[30,52−56]

DOI: 10.1021/jacs.6b10731
J. Am. Chem. Soc. 2017, 139, 2981−2988

Here, a total of 12 replicate MDS were carried out wherein a SP^{3+} peptide ion was placed at the center of a water droplet with a net charge of 15+, achieved by the addition of 22 H_3O^+ and 10 Cl^- ions randomly dispersed within the droplet. Figure 1 shows snapshots from a representative simulation illustrating the observed events in the first 2 ns of desolvation. Early in the evolution of the droplet, water evaporation and water/hydronium cluster ejection dominate the desolvation process (see Figures 1A and 1**B**); however, some of the hydronium and chloride ions also migrate to the droplet surface resulting in droplet distortion and formation of "spiky protrusions", as noted previously by Consta et al.[19,52,57] As the droplet shrinks and the charge on the droplet surpasses the Rayleigh limit, fission of these lobes carry away hydronium and chloride ions (Figure 1C). Following these fission events, the droplet regains a more spherical shape (Figure 1D), and water evaporation once more dominates the desolvation process. Upon further reduction in droplet size by evaporation, the surface charge on the droplet once more approaches the Rayleigh limit, resulting in an additional droplet fission event (Figure 1E), after which water evaporation resumed. The final product of droplet fission and dehydration is a complex that is composed of SP^{3+}, H_3O^+, Cl^-, and a few molecules of H_2O (structure I), which is consistent with the CRM mechanism described by Consta et al.[19] and Konermann et al.[20] Note also that the shapes ("spiky protrusions") of the droplets, especially those shown in panel C, are very similar to those reported previously.[58] The process of droplet fission/evaporation as shown in Figure 1 was observed in all other replicate desolvation simulations.

Structure I

MD Simulations of the Effects of Fission/Dehydration on the Conformation of the SP^{3+} Ion. Figure 2 shows the results of three representative simulations of the 12 performed on SP^{3+} in this study (results of all 12 replicate simulations are shown in Figure S7). Figure 2A, 2B, and 2C show changes in the calculated CCS values and conformational preferences (i–iv) for a SP^{3+} ion as the number of water molecules in the droplet changes as a function of time. Note that the starting structures for the SP^{3+} ions in Figure 2A-i and 2B-i are fully elongated structures having a calculated CCS of 420 $Å^2$, whereas the starting structure of SP^{3+} in Figure 2C-i is a compact conformer having a CCS ≈ 320 $Å^2$ that is similar to conformer A (316 $Å^2$) reported by Silveira et al.[31,48] The most notable aspect of these simulations is that Cl^- and H_3O^+ ion interactions with water and the peptide ion play important roles in defining the conformational preference of the solvent-free, gas-phase peptide ion. For example, as the numbers of water molecules decrease, both H_3O^+ and Cl^- ions cluster around the protonated N-terminus and R and K side chains of the SP^{3+} ion. Consta et al. reported similar simulations for a PEG molecule in a droplet containing Na^+ and Cl^- ions. PEG-anion adducts were not observed owing to the absence of anion binding sites on the PEG molecule, but they noted that the presence of counterions had an indirect impact on the charge state and formation of PEG Na^+ adduct ions.[56] Konermann et al. reported simulation studies for an ESI droplet containing a protein (ubiquitin, cytochrome C, or holomyoglobin) and Na^+ and Cl^- ions, and they noted minimal impact on the protein structure after droplet desolvation;[30] however, in these studies, the detailed inter/intramolecular interactions involving the small ions and the protein were not probed in depth. The following discussion focuses on the changes in the conformation of the SP^{3+} ion that occur as a result of reduction in the droplet size as well as the presence of H_3O^+ and Cl^- ions.

During the early stages of each simulation (~300 ps), SP^{3+} ions adopt a distribution of conformations that have CCS values centered around ~395 $Å^2$, independent of the initial conformation (see representative structures in Figures 2A-ii, 2B-ii, and 2C-ii). This CCS value of ~395 $Å^2$ is consistent with the calculated CCS from the PDB structure (2KS9) reported from solution phase NMR studies.[59] Under these conditions the hydration layer for peptides corresponds to multiple solvation shells, which should closely approximate a "bulk-like" solvent environment.[60] The convergence to a CCS of ~395 $Å^2$ can be attributed to conformational equilibration from initial non-native structures to bulk-like, solution-phase structures, especially for the elongation of the compact starting conformer for Figure 2C-i. Upon further reduction in droplet size the hydrophobic side chains migrate to the droplet surface, which leads to coiling of the hydrophobic C-terminal region (see representative structures in Figure 2A-iii, 2B-iii, and 2C-iii). After this coiling event, the hydrophobic region remains desolvated as shown in Figure 2. During the early stages of the simulations, intermolecular interactions between the counterions and the SP^{3+} ions are transient such that the counterions and polar residues of the peptide are solvated by the water. Upon further droplet shrinkage by water evaporation, ion–ion intermolecular and peptide intramolecular charge solvation exhibits increasing influence on the conformational preference of the peptide. The CCS of the final structures shown in Figure 2A-iv, 2B-iv, and 2C-iv are within 4% of the experimentally determined value of 316 $Å^2$ for the compact conformer, previously denoted as conformer A.[31,48] It has been previously reported that intramolecular charge solvation involving the charge-carrying N-terminus, arginine (R1), lysine (K3), and the polar glutamines (Q5 and Q6) is essential for preserving the kinetically trapped SP^{3+} ion conformer A;[31,48] the final structures obtained from these simulations exhibit multiple intramolecular interactions that define the conformation of the desolvated peptide ion. Furthermore, in each case the H_3O^+ and Cl^- ions are clustered around the N-terminal region of the peptide, which suggests that these interactions diminish charge solvation by the glutamine side chains.

Although the general trends observed in the simulations shown in Figure 2 are apparent in each of the 12 simulations, there are several noteworthy variations. For example, early in the simulation shown in Figure 3A and 3B the CCS for SP^{3+} ions begins to converge to more compact conformers (Figure 3A-i and 3B-i); however, these conformers are short-lived and rather quickly rearrange to extended conformers. Also, late in the desolvation process the trajectory shown in Figure 3A does not show evidence of convergence to a compact conformer, whereas Figure 3B does show evidence for convergence to a compact conformer. It appears that the structural transitions that occur in these intermediate regions may involve independent pathways for forming compact conformers as well as extended conformers (368 $Å^2$), the latter being products of the dehydration observed in the cryo-IM-MS experiment.

DOI: 10.1021/jacs.6b10731
J. Am. Chem. Soc. 2017, 139, 2981–2988

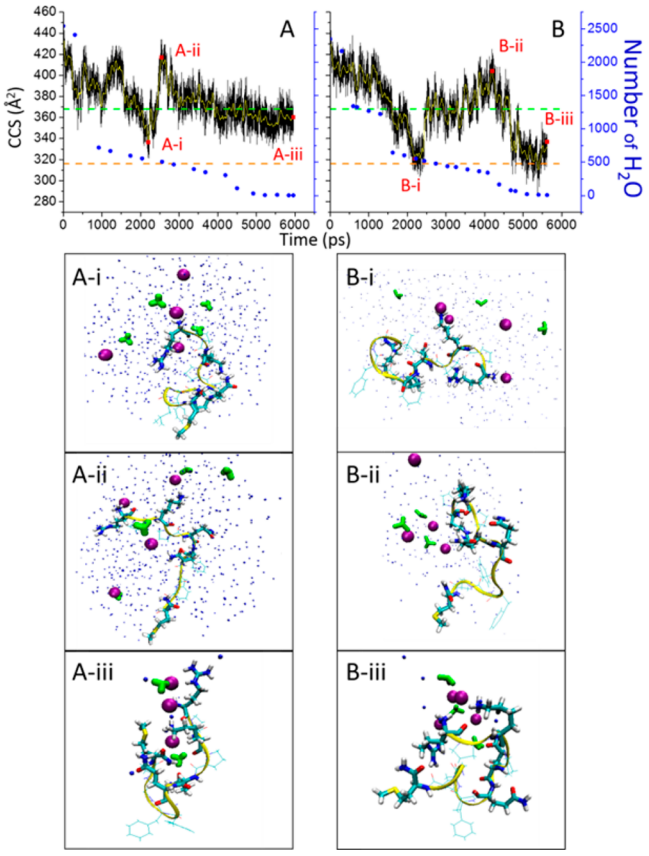

Figure 3. (A and B) Two plots showing the (raw data, black line; smoothed, yellow line) CCS of SP^{3+} ions and (blue points) numbers of water molecules vs time extracted from selected simulations. The experimentally determined CCS of SP^{3+} (316 $Å^2$ orange dash and 368 $Å^2$, green dash) is also shown for reference. Structures labeled as i–iii depict representative snapshots of the simulations (A and B): (i) the postfission compact structures observed at ~2000 ps, (ii) the elongated structures observed later in the simulation, and (iii) the final frame of the desolvation simulation. Blue dots represent water molecules, purple spheres represent chloride ions, and hydronium ions are shown in green.

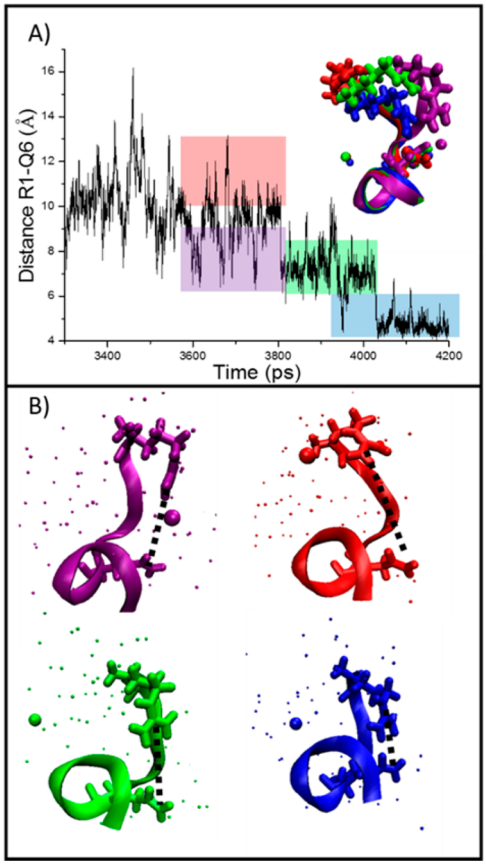

Figure 4. (A) Distance plot between $R1C^{\zeta}$ and $Q6C^{\delta}$ during the time period 3300 to 4200 ps for the simulated results presented in Figure 2A, and (B) representative structures determined by K-clust algorithm for the color-coded regions for the trajectory shown in (A). Water molecules are shown as small dots. A single Cl^- ion is shown as the large sphere; the other Cl^- ions are not shown because they do not appear to influence the $R1C^{\zeta}$ and $Q6C^{\delta}$ distance. The distance between the two carbon atoms of interest are labeled with black dashed lines. Structures are color coded with respect to the colored regions in panel (A).

The differences in the final structures observed for the simulations shown in Figure 3A and 3B are attributed to differences in counterion interactions during the late stages of dehydration. At the end of the simulation shown in Figure 3A-iii, the H_3O^+ and Cl^- ions are dispersed along the peptide backbone between the two strands of a turn-type structure, thereby inhibiting intramolecular charge solvation previously shown to favor formation of a compact conformer.[31,48] However, at the end of the simulation shown in Figure 3B-iii, H_3O^+ and Cl^- ions are clustered around the N-terminus, as shown in Figure 2, and the charged and polar glutamine side chains are still free to participate in intramolecular charge solvation interactions that favor formation of compact conformers.

Overall, the simulations shown in Figures 2 and 3 illustrate the influence of inter-/intramolecular charge solvation interactions between SP^{3+}, Cl^-, H_3O^+, and H_2O to the final conformational preference of the peptide. Different types of interactions observed in the simulations are illustrated in Figure 4. Figure 4A contains a plot of the distance between the R1 guanidinium group carbon atom ($R1C^{\zeta}$) and the Q6 side-chain terminal carbon atom ($Q6C^{\delta}$) for the simulation reported in Figure 2A. The colored structures shown in Figure 4B correspond to the colored regions of the plot in Figure 4A. The purple structure denotes SP^{3+} when the distance between $R1C^{\zeta}$ and $Q6C^{\delta}$ is less than 9 Å and a chloride ion and water molecule form a bridge between the protons on the guanidinium ion and the Q6 side chain amide group. When the chloride ion moves out of the bridging interaction, the distance between R1 and Q6 is >9 Å. The distance plot indicates that SP^{3+} interconverts between the two structures represented by purple and red. One such conversion results in the guanidinium group forming a bridge involving a single water molecule to the glutamine side chain; note the chloride ion has remained at the N-terminus and/or near the K3 side chain. The chloride ion binds more strongly to the ammonium ion of lysine and the N-terminus rather than the guanidinium ion of arginine owing to the more diffuse charge. The final transition occurs when the remaining water molecule is removed, intramolecular charge solvation is dominant, and the $R1C^{\zeta}$–$Q6C^{\delta}$ distance is <5 Å resulting in a structure represented in the blue. Later in the simulation, the guanidinium ion is charge solvated by multiple backbone carbonyl groups, which also results in formation of a compact conformer. The intramolecular charge solvation of the guanidinium ion is preserved until the end of the simulation (the structure is shown in Figure 2A-iv). Overall, these changes in intramolecular charge solvation suggest that the position of Cl^- ions indirectly affects conformational

DOI: 10.1021/jacs.6b10731
J. Am. Chem. Soc. 2017, 139, 2981–2988

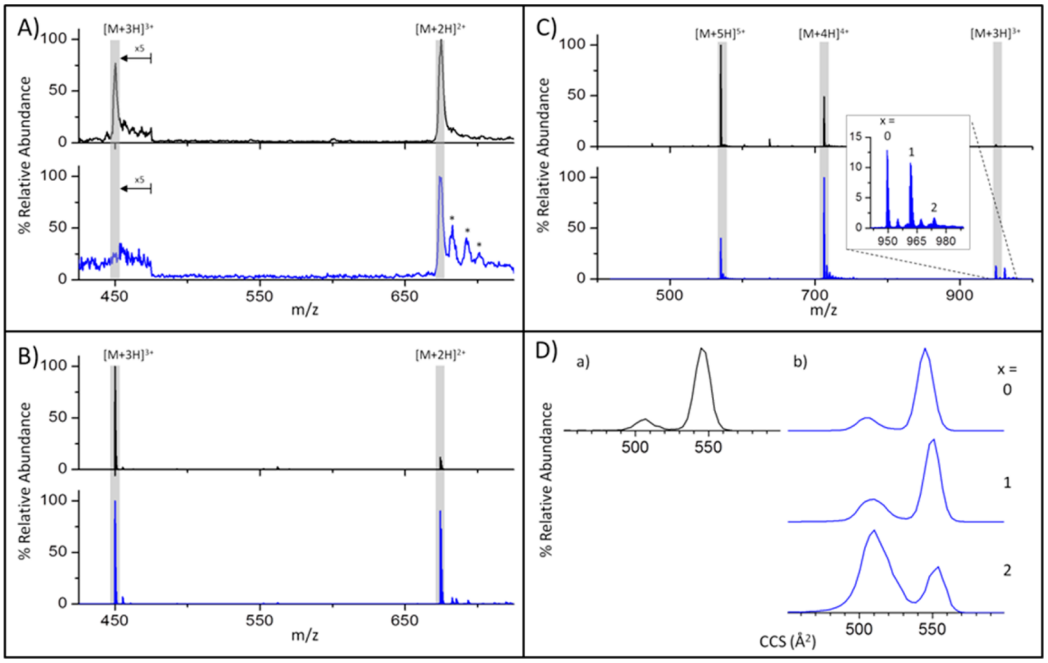

Figure 5. (A) The ESI-mass spectra acquired using cryo-MS of SP sprayed from water/0.1% formic acid (top, black) and water/0.1% HCl (bottom, blue) showing the decrease in charge induced by the presence of Cl^- adducts. Note that the mass spectrum for m/z less than 475 is amplified by five to better show the $[M + 3H]^{3+}$ ion and starred peaks are not adduct peaks but instead correspond to a 16 Da mass increase, likely the product of methionine oxidation. (B) The ESI-mass spectra acquired under ambient conditions of SP sprayed from water (top, black) and water/0.1% HCl (bottom, blue) showing the decrease in charge induced by the presence of Cl^- adducts. (C) The ESI-mass spectra of melittin (GIGAVLKVLTTGLPALIS-WIKRKRQQ-NH_2) acquired under ambient conditions resulting from water (top, black) and water/0.1% HCl (bottom, blue). Chloride-adducted melittin, $[M + nH + xCl]^{(n-x)+}$, is observed with a total charge of 3+ when HCl is added to the sample solution (see inset for ions where $x = 0-2$). (D) CCS profiles observed for melittin $[M + 3H]^{3+}$ ions electrosprayed from water (i) and $[M + nH + xCl]^{3+}$ ions electrosprayed from water/0.1% HCl (ii). Each $[M + nH + xCl]^{3+}$ ion in (ii) is labeled for the number of chloride adducts ($x = 0-2$).

preferences—had the Cl^- not relocated to the N-terminal region of the peptide prior to the final stages of evaporation, the peptide could not have formed a compact conformer. The final structures from each simulation indicate that a few water molecules remain bound to the SP^{3+} ion; however, it is important to note that the water molecules have lost all bulk-solvent characteristics and as such function as an adduct. Similarly to that reported previously, water adducts have minimal impact on the conformational preference of the biomolecule.[27]

Our previous SP paper showed evidence that intramolecular interactions involving the glutamines (Q5 and Q6) are responsible for formation of the compact conformer; i.e., the compact conformer is destabilized for the Q5A, Q6A, and Q5,6A mutants, and to a much lesser extent for F7A, F8A, and/or C-terminal mutation.[48] The data presented herein support the identification of intramolecular interactions between the charged residues and Q5, Q6, F7, F8, and the C-terminus as integral to producing a compact conformer in that such interactions were observed in all simulation results producing a compact conformer. These residues provide charge solvation as the droplet decreases in size; an example of such an interaction is shown as the blue structure in Figure 4B. However, the final compact structures exhibit a variety of intramolecular interactions that may or may not include Q5, Q6, F7, F8, or the C-terminus.

In total, 12 desolvation simulations were performed (full CCS maps are shown in Figure S9). Those simulations that form compact desolvated conformations have demonstrated that the desolvated compact peptide ion is stabilized via multiple intramolecular interactions involving some combination of the N-terminus, C-terminus, R1, K3, Q5, Q6, and backbone carbonyl groups. In addition, the formation of these intramolecular interactions is more likely when the counterions migrate and assemble on the N-terminal region of SP^{3+}.

Effects of Chloride Anions on Dehydration and Conformation of SP^{3+} Ions. Anion adduction to ESI product ions has been shown to exhibit significant effects on charge state distributions, protein conformational preference, and protein complex stability.[61−65] Of specific relevance to this study, a recent study has shown that Cl^-, H_2O, and H_3O^+ adducted protein ions are observed using ambient ESI mass spectra if care is taken to minimize collisional activation, and the adducted Cl^- ions played a direct role in defining the conformational preference of a desolvated protein ion.[65] Although the simulations presented in this study suggest that interactions between hydrated SP^{3+} and Cl^- ions are retained until the final stages of ESI droplet evaporation, the ESI mass spectra of SP in 0.1% HCl acquired using both cryogenic (Figure 5A) and ambient (Figure 5B) MS show no evidence of peptide−chloride, −hydronium, or −water clusters. Despite this absence of explicit peptide−chloride adduct ions in the mass spectra, there is indirect evidence that the presence of Cl^- influences the ESI process. For example, the abundances of $[M + 3H]^{3+}$ and $[M + 2H]^{2+}$ ions in the mass spectra of SP sprayed from pure water, 0.1% formic acid, and 0.1% HCl solutions are quite different. Specifically the abundance of SP^{3+} is attenuated relative to SP^{2+} ions from solutions containing formic acid and HCl (Figure 5A−B), which is a direct result of formate and Cl^- ion-induced charge reduction as noted previously by Mirza and Chait.[61] Possible mechanisms by which charge reduction reactions occur have

DOI: 10.1021/jacs.6b10731
J. Am. Chem. Soc. 2017, 139, 2981−2988

been suggested. For the specific case of 0.1% HCl solutions, we interpret these results as evidence that Cl^- adduct ions are retained upon complete desolvation, but subsequent reactions leading to loss of Cl^-, HCl, and/or $H^+(H_2O)_nCl^-$ are favored in the gas phase.[61,65−67] This hypothesis was further tested by examining the effects of Cl^- ions on the ESI product ion yield for the amphipathic peptide melittin. In the case of melittin we observed both the products of charge reduction reactions as well as peptide−Cl^- adduct ions, specifically $[M + nH + xCl]^{(n-x)+}$ (Figure 5C). The differences between the mass spectra of SP and melittin are attributed to the higher number of hydrophilic amino acid side chains, which increases the overall number of charge carriers as well as anion binding sites. Note that the cryo-MS instrument lacks sufficient mass resolution to differentiate the presence of two H_2O molecule adducts from that for a chloride adduct, especially with increasing charge; consequently, the ESI mass spectra reported for melittin (Figure 5C) were acquired using a high resolution instrument under ambient conditions.

The MD simulations for SP^{3+} ions suggest that the location of counterions adducted to the peptide could influence the conformational preference of the desolvated peptide. The experimental CCS profiles for the protonated SP and melittin ions electrosprayed from water and water/0.1% HCl solutions are indistinguishable; however, the abundances of the compact conformers are higher for the melittin−Cl^- adduct ions (Figure 5D). Melittin has been the subject of several ion mobility studies.[68−71] The reported solution-phase structure of melittin consists of two α helices connected by a short flexible hinge region.[72] Florance et al. reported a single CCS value of 544 $Å^2$ for the $[M + 3H]^{3+}$ ion.[70] More recently, May and McLean[71] have shown that the $[M + 3H]^{3+}$ ions are composed of three conformer families, compact (CCS ≈ 410 $Å^2$), intermediate (CCS ≈ 485 $Å^2$), and extended (CCS ≈ 515 $Å^2$) conformers. The observed CCS profiles for $[M + 3H]^{3+}$ ions (Figure 5D) indicate two distinct conformer populations, similar to those reported.[70,71] A small increase in the abundance of the compact conformer for the $[M + 4H + 1Cl]^{3+}$ ion is observed, but an even larger increase in the abundance of the compact conformer is observed for $[M + 5H + 2Cl]^{3+}$ ions. This preference for a compact conformer of chloride-adducted melittin is consistent with previously published results.[65]

CONCLUSIONS

MD simulations of the dehydration of ESI-formed droplets containing a SP^{3+} ion, chloride counterions, and hydronium ions yield new insights into peptide ion conformational changes in the final stages of dehydration. Combining the results of MD simulation with those from cryo-IM-MS affords new insights about the effects of decreasing droplet size and increasing concentration of H_3O^+ and Cl^- (and other counteranions) on the conformational evolution of an amphipathic peptide. The changes in the CCS of the SP^{3+} ion and the peptide structure reveal that the droplet volume primarily dictates the structure of the SP^{3+} ion. When fully immersed in the water droplet, SP^{3+} ions favor an extended conformation that is similar to that reported by Silveira et al.[31,33,48] and the solution-phase structure reported by Gayen et al.[59] As the droplet shrinks, the hydrophobic C-terminus migrates to the droplet surface. Upon further dehydration inter/intramolecular charge solvation of the charge sites becomes increasingly prevalent and these interactions define the final conformational preference of the desolvated SP^{3+} ions. Although several of the simulations did not yield a compact conformer for the desolvated SP^{3+} ion, this appears to be a result of alternative charge solvation interactions involving H_3O^+ and Cl^- ions that impede intramolecular interactions that favor formation of an extended conformer. Despite the transient role of water in the formation of intramolecular interactions, the final few water molecules remaining bound to the peptide ion demonstrate minimal effect on the peptide conformational preference. This can be explained by the loss of bulk solvent characteristics; the remaining water molecules function as a simple adduct, suggesting that the peptide ion is effectively "solvent-free." In summary, SP conformational preference changes dramatically over the course of the ESI process, multiple intramolecular interactions between charged sites and polar sites on the peptide are necessary to form compact conformers with CCS values consistent with the kinetically trapped compact conformer,[48] and the interruption of these intramolecular interactions through intermolecular charge solvation can inhibit formation of the compact conformer.

It is apparent from MD simulations that the peptide−cation/anion cluster survives until the final stages of the desolvation process; however, these clusters are notably absent from the ESI-MS spectra of SP electrosprayed from HCl acidified solutions. Although the observed charge reduction suggests that peptide−cation/anion clusters survive the desolvation process, these ions do not survive transmission through the instrument. Instead, the clusters undergo reactions that are best described as gas-phase ion/ion reaction chemistry.[73] This explanation is supported by results obtained from ESI-IM-MS of melittin, viz. the observed chloride adduct ions and charge reduction product ions. Overall, these MD simulations provide unique insight into key microscopic events occurring throughout the desolvation of electrosprayed peptide ions and counterions and the inter/intramolecular interactions that influences the conformational preferences.

ASSOCIATED CONTENT

Supporting Information

The Supporting Information is available free of charge on the ACS Publications website at DOI: 10.1021/jacs.6b10731.

Preliminary simulation results with different temperatures, numbers of charge, and electrostatic nonbonding cutoff on simulated droplet fission events, solvent evaporation, and overall droplet dynamics (PDF)

AUTHOR INFORMATION

Corresponding Author

*russell@chem.tamu.edu

ORCID

David H. Russell: 0000-0003-0830-3914

Present Address

§Department of Chemistry & Biochemistry, Texas Tech University, Lubbock, TX 79409.

Notes

The authors declare no competing financial interest.

ACKNOWLEDGMENTS

Funding for this work was provided by the U.S. Department of Energy Office of Science, Basic Energy Sciences (BES DE-FG02-04ER15520). The National Science Foundation (Grant No. CHE-0541587) provided funding for the simulations.

DOI: 10.1021/jacs.6b10731
J. Am. Chem. Soc. 2017, 139, 2981−2988

REFERENCES

(1) Heuvel, R. H. H. v. d.; Heck, A. J. R. *Curr. Opin. Chem. Biol.* **2004**, *8*, 519.
(2) Uetrecht, C.; Rose, R. J.; van Duijn, E.; Lorenzen, K.; Heck, A. J. R. *Chem. Soc. Rev.* **2010**, *39*, 1633.
(3) Chait, B. T.; Cadene, M.; Olinares, P. D.; Rout, M. P.; Shi, Y. *J. Am. Soc. Mass Spectrom.* **2016**, *27*, 952.
(4) Loo, J. A. *Mass Spectrom. Rev.* **1997**, *16*, 1.
(5) Loo, J. A. *Int. J. Mass Spectrom.* **2000**, *200*, 175.
(6) Breuker, K.; McLafferty, F. W. *Proc. Natl. Acad. Sci. U. S. A.* **2008**, *105*, 18145.
(7) Wyttenbach, T.; Bowers, M. T. *J. Phys. Chem. B* **2011**, *115*, 12266.
(8) Shi, H.; Atlasevich, N.; Merenbloom, S.; Clemmer, D. *J. Am. Soc. Mass Spectrom.* **2014**, *25*, 2000.
(9) Chen, S.-H.; Russell, D. *J. Am. Soc. Mass Spectrom.* **2015**, *26*, 1433.
(10) Chen, S.-H.; Chen, L.; Russell, D. H. *J. Am. Chem. Soc.* **2014**, *136*, 9499.
(11) Fenn, J.; Mann, M.; Meng, C.; Wong, S.; Whitehouse, C. *Science* **1989**, *246*, 64.
(12) Gomez, A.; Tang, K. *Phys. Fluids* **1994**, *6*, 404.
(13) Cech, N. B.; Enke, C. G. *Mass Spectrom. Rev.* **2001**, *20*, 362.
(14) Kebarle, P.; Verkerk, U. H. *Mass Spectrom. Rev.* **2009**, *28*, 898.
(15) Hamdy, O.; Julian, R. *J. Am. Soc. Mass Spectrom.* **2012**, *23*, 1.
(16) Dole, M.; Mack, L. L.; Hines, R. L.; Mobley, R. C.; Ferguson, L. D.; Alice, M. B. *J. Chem. Phys.* **1968**, *49*, 2240.
(17) Gamero-Castaño, M.; Mora, J. F. d. l. *J. Mass Spectrom.* **2000**, *35*, 790.
(18) Gamero-Castaño, M.; Fernández de la Mora, J. *Anal. Chim. Acta* **2000**, *406*, 67.
(19) Consta, S.; Oh, M. I.; Malevanets, A. *Chem. Phys. Lett.* **2016**, *663*, 1.
(20) Konermann, L.; Ahadi, E.; Rodriguez, A. D.; Vahidi, S. *Anal. Chem.* **2013**, *85*, 2.
(21) Iavarone, A. T.; Williams, E. R. *J. Am. Chem. Soc.* **2003**, *125*, 2319.
(22) Iribarne, J. V.; Thomson, B. A. *J. Chem. Phys.* **1976**, *64*, 2287.
(23) Fernandez de la Mora, J. *Anal. Chim. Acta* **2000**, *406*, 93.
(24) Hogan, C. J.; Carroll, J. A.; Rohrs, H. W.; Biswas, P.; Gross, M. L. *Anal. Chem.* **2009**, *81*, 369.
(25) Consta, S.; Malevanets, A. *Phys. Rev. Lett.* **2012**, *109*, 148301.
(26) Ahadi, E.; Konermann, L. *J. Phys. Chem. B* **2012**, *116*, 104.
(27) Konermann, L.; Rodriguez, A. D.; Liu, J. *Anal. Chem.* **2012**, *84*, 6798.
(28) Steinberg, M. Z.; Breuker, K.; Elber, R.; Gerber, R. B. *Phys. Chem. Chem. Phys.* **2007**, *9*, 4690.
(29) Soltani, S.; Oh, M. I.; Consta, S. *J. Chem. Phys.* **2015**, *142*, 114307.
(30) McAllister, R. G.; Metwally, H.; Sun, Y.; Konermann, L. *J. Am. Chem. Soc.* **2015**, *137*, 12667.
(31) Silveira, J. A.; Fort, K. L.; Kim, D.; Servage, K. A.; Pierson, N. A.; Clemmer, D. E.; Russell, D. H. *J. Am. Chem. Soc.* **2013**, *135*, 19147.
(32) Servage, K. A.; Fort, K. L.; Silveira, J. A.; Shi, L.; Clemmer, D. E.; Russell, D. H. *J. Am. Chem. Soc.* **2015**, *137*, 8916.
(33) Servage, K. A.; Silveira, J. A.; Fort, K. L.; Russell, D. H. *J. Phys. Chem. B* **2015**, *119*, 4693.
(34) Servage, K. A.; Silveira, J. A.; Fort, K. L.; Russell, D. H. *Acc. Chem. Res.* **2016**, *49*, 1421.
(35) Dupradeau, F.-Y.; Zaffran, A. P.; Savineau, C.; Lelong, R.; Grivel, N.; Lelong, D.; Rosanski, W.; Cieplak, P. *Phys. Chem. Chem. Phys.* **2010**, *12*, 7821.
(36) Baaden, M.; Burgard, M.; Wipff, G. *J. Phys. Chem. B* **2001**, *105*, 11131.
(37) Shvartsburg, A. A.; Jarrold, M. F. *Chem. Phys. Lett.* **1996**, *261*, 86.
(38) Mesleh, M. F.; Hunter, J. M.; Shvartsburg, A. A.; Schatz, G. C.; Jarrold, M. F. *J. Phys. Chem.* **1996**, *100*, 16082.
(39) Jorgensen, W. L.; Chandrasekhar, J.; Madura, J. D.; Impey, R. W.; Klein, M. L. *J. Chem. Phys.* **1983**, *79*, 926.
(40) Vega, C.; de Miguel, E. *J. Chem. Phys.* **2007**, *126*, 154707.
(41) Marginean, I.; Znamenskiy, V.; Vertes, A. *J. Phys. Chem. B* **2006**, *110*, 6397.
(42) Konermann, L.; McAllister, R. G.; Metwally, H. *J. Phys. Chem. B* **2014**, *118*, 12025.
(43) Peng, Y.; Swanson, J. M. J.; Kang, S.-g.; Zhou, R.; Voth, G. A. *J. Phys. Chem. B* **2015**, *119*, 9212.
(44) Jungwirth, P.; Tobias, D. J. *Chem. Rev.* **2006**, *106*, 1259.
(45) Caleman, C.; van der Spoel, D. *J. Chem. Phys.* **2006**, *125*, 154508.
(46) Wilm, M. *Mol. Cell. Proteomics* **2011**, *10*, M111.009407.
(47) Bleiholder, C.; Suhai, S.; Paizs, B. *J. Am. Soc. Mass Spectrom.* **2006**, *17*, 1275.
(48) Fort, K. L.; Silveira, J. A.; Pierson, N. A.; Servage, K. A.; Clemmer, D. E.; Russell, D. H. *J. Phys. Chem. B* **2014**, *118*, 14336.
(49) Silveira, J. A.; Servage, K. A.; Gamage, C. M.; Russell, D. H. *J. Phys. Chem. A* **2013**, *117*, 953.
(50) Servage, K. A.; Silveira, J. A.; Fort, K. L.; Russell, D. H. *J. Phys. Chem. Lett.* **2014**, *5*, 1825.
(51) May, J. C.; Russell, D. H. *J. Am. Soc. Mass Spectrom.* **2011**, *22*, 1134.
(52) Sharawy, M.; Consta, S. *Phys. Chem. Chem. Phys.* **2015**, *17*, 25550.
(53) Consta, S.; Kapral, R. *J. Chem. Phys.* **1999**, *111*, 10183.
(54) Malevanets, A.; Consta, S. *J. Chem. Phys.* **2013**, *138*, 184312.
(55) Paliy, M.; Consta, S.; Yang, J. *J. Phys. Chem. C* **2014**, *118*, 16074.
(56) Sharawy, M.; Consta, S. *J. Chem. Phys.* **2014**, *141*, 104321.
(57) Sharawy, M.; Consta, S. *J. Phys. Chem. A* **2016**, *120*, 8871.
(58) Consta, S. *J. Phys. Chem. B* **2010**, *114*, 5263.
(59) Gayen, A.; Goswami, S. K.; Mukhopadhyay, C. *Biochim. Biophys. Acta, Biomembr.* **2011**, *1808*, 127.
(60) Cooper, R. J.; DiTucci, M. J.; Chang, T. M.; Williams, E. R. *J. Am. Chem. Soc.* **2016**, *138*, 96.
(61) Mirza, U. A.; Chait, B. T. *Anal. Chem.* **1994**, *66*, 2898.
(62) Merenbloom, S.; Flick, T.; Daly, M.; Williams, E. *J. Am. Soc. Mass Spectrom.* **2011**, *22*, 1978.
(63) Han, L.; Hyung, S.-J.; Mayers, J. J. S.; Ruotolo, B. T. *J. Am. Chem. Soc.* **2011**, *133*, 11358.
(64) Chang, T. M.; Berden, G.; Oomens, J.; Williams, E. R. *Int. J. Mass Spectrom.* **2015**, *377*, 440.
(65) Wagner, N. D.; Kim, D.; Russell, D. H. *Anal. Chem.* **2016**, *88*, 5934.
(66) Liu, X.; Cole, R. *J. Am. Soc. Mass Spectrom.* **2011**, *22*, 2125.
(67) Mancini, J. S.; Bowman, J. M. *Phys. Chem. Chem. Phys.* **2015**, *17*, 6222.
(68) Figueroa, I. D.; Torres, O.; Russell, D. H. *Anal. Chem.* **1998**, *70*, 4527.
(69) Figueroa, I.; Russell, D. *J. Am. Soc. Mass Spectrom.* **1999**, *10*, 719.
(70) Florance, H. V.; Stopford, A. P.; Kalapothakis, J. M.; McCullough, B. J.; Bretherick, A.; Barran, P. E. *Analyst* **2011**, *136*, 3446.
(71) May, J. C.; McLean, J. A. *Proteomics* **2015**, *15*, 2862.
(72) Bazzo, R.; Tappin, M. J.; Pastore, A.; Harvey, T. S.; Carver, J. A.; Campbell, I. D. *Eur. J. Biochem.* **1988**, *173*, 139.
(73) McLuckey, S. A.; Huang, T.-Y. *Anal. Chem.* **2009**, *81*, 8669.

DOI: 10.1021/jacs.6b10731
J. Am. Chem. Soc. 2017, 139, 2981−2988